CFD Simulation of a Heated Round Jet of Sodium (TEFLU Benchmark)

S. Buono, L. Maciocco, V. Moreau, L. Sorrentino

17 July 2001

Abstract

The results of the numerical simulation of a heated sodium round jet in a co-flow (TEFLU experiments) are presented for three different flow regimes (forced flow, buoyant flow and plume), and compared with experimental results.

The main aim of this work was the analysis of the applicability of a turbulent-Prandtl-number approach for the modelling of the turbulent transport of energy in the case of fluids with very low molecular Prandtl number (liquid metals). All the calculations were performed with the Star-CD finite-volume commercial code.

The forced flow case was considered first. A comparison among different k-ε turbulence models implemented in Star-CD was carried out. The Chen k-ε model gave the best agreement with experimental results.

A study of the influence of the turbulent Prandtl number Pr_t was then carried out. The first step was the comparison between the molecular conductivity and the turbulent heat diffusion coefficients, calculated using the turbulent Prandtl number approach (Reynolds analogy). It was found that that the two contributions are of the same order of magnitude. This result implies that there is a strong interaction between the molecular and turbulent heat transfer, which could have a strong effect on the scaling coefficient between the turbulent transfer of momentum and heat, namely on Pr_t.

In order to study the effect of the variation of Pr_t on the temperature profiles, the inlet turbulence kinetic energy profile was scaled in order to obtain a good agreement between calculated and experimental velocity profiles. Then, the value of Pr_t was changed from the standard value of 0.9 to 10 and to 10^4 (to exclude the contribution of the turbulent heat transfer). A very good agreement with experimental measurements was found in both cases (the best being the case of no turbulent heat transfer).

On the basis of the results obtained in the forced-flow case, the cases of buoyant flow and plume were simulated, getting substantially the same results.

The above results indicate that the heat conduction is predominant in all flow regimes. In this situation, the standard value 0.9 of Pr_t yields an overestimation of the thermal diffusion rate.

Contents

1 Introduction 3
2 Test case set-up 4
2.1 Description 4
2.2 Numerical set-up and boundary conditions 5
3 Forced-flow simulations 8
3.1 Comparison between the two options of extrapolated and imposed ε boundary condition 8
3.2 Calculation with the Chen k-ε and comparison with other k-ε models implemented in Star-CD 9
3.3 Analysis of the influence of the value of the turbulent Prandtl number 11
4 Simulations of buoyant flow and plume regimes 16
4.1 Buoyant flow 16
4.2 Plume 18
5 Conclusions 20
6 References 21

1 Introduction

The TEFLU experiments [1] were performed at the Karlsruhe Research Centre (FZK) in order to study the thermal-fluid dynamic behaviour of a hot sodium jet in different flow regimes. It was chosen by the Benchmark Working Group (BWG) on Heavy Liquid Metals (HLMs) [2] as a benchmark for testing the capabilities of Computational Fluid Dynamics (CFD) codes at simulating HLM turbulent flows with heat transfer.

In all two-equations turbulence models (which are the most commonly used in industrial CFD simulations), as well as in the Reynolds Stress model, the turbulent heat transport is modelled on the basis of an analogy with the turbulent transport of momentum (Reynolds analogy, see [6] for a simple description of the turbulence models implemented in Star-CD). In fact, the turbulent heat diffusion coefficient is assumed to be proportional to the turbulent viscosity through an empirical constant (the turbulent Prandtl number Pr_t).

On the basis of the experience with fluids with Prandtl number of order unity, this coefficient is usually set to a value of 0.9, which means that turbulent transport of momentum and heat are almost equivalent. However, for fluids with low Prandtl number (i.e. high thermal molecular diffusivity with respect to the molecular viscosity), this value could be incorrect. An expression relating Pr_t to the Prandtl and Reynolds number has been deduced by Jisha and Rieke on the basis of theoretical and empirical considerations [7].

Beside the problem of Pr_t, which is mainly related to the simulation of liquid metal flows, two more difficulties arise in the simulation of the TEFLU benchmark. The first concerns the intrinsic limitations of turbulence models, which are related to the type of flow to be simulated. The second is related to the inlet boundary conditions for the turbulence parameters.

It is well known that almost all the various versions of two-equations models give rise to the so-called round-jet anomaly [10]. In fact, the Standard and RNG k-ε models as well as the k-ω model, predict a too high jet spreading-rate. The problem is faced in the Chen k-ε model [5], through the introduction of a new term (the dissipation time scale) in the ε equation.

The TEFLU experimental apparatus allowed the measurement of velocity, temperature and temperature fluctuations. No experimental data are available for velocity fluctuations. This is a problem for the definition of turbulence boundary conditions for the numerical simulation, which makes the evaluation of the capability of turbulence models at predicting the correct jet spreading rate quite questionable.

Despite the above-mentioned problems, some conclusions can nevertheless be drawn from the TEFLU benchmark, as described further on.

2 Test case set-up

2.1 Description

The sketch of the TEFLU benchmark is shown in Figure 1, where the calculation domain is traced with bold lines. Sodium physical properties are reported in Table 1.

The considered flow regimes are listed in Table 2, where the subscripts cf and j refer to co-flow and jet characteristics respectively, and Δu_j and ΔT_j are the difference between the jet and the co-flow velocity and temperature, namely

$$\Delta \bar{u}_j = \bar{u}_j - \bar{u}_{cf} \tag{1}$$

$$\Delta \bar{T}_j = \bar{T}_j - \bar{T}_{cf} \tag{2}$$

The following number are also defined:

$$Re_{cf} = \frac{\bar{u}_{cf} D}{\nu_0}$$ co-flow Reynolds number

$$Re_j = \frac{\bar{u}_j d}{\nu_0}$$ jet Reynolds number

$$Fr_j = \frac{\rho_j(\overline{u_j^2} - \bar{u}_{cf}^2)}{g(\rho_{cf} - \rho_j)d}$$ densimetric Froude number

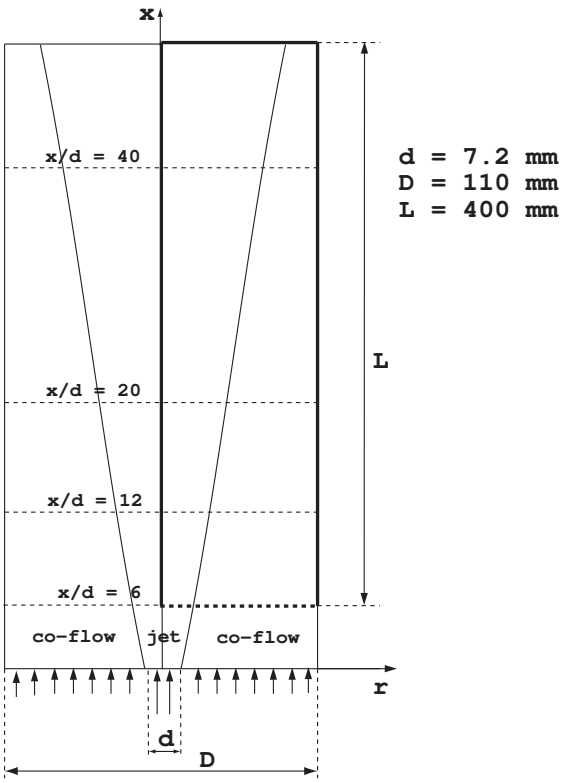

Figure 1: sketch of the TEFLU test case. The calculation domain is traced with bold lines.

Property	Symbol [units]	Value for T = 300 °C
Density	ρ [Kg/m^3]	880
Thermal conductivity	λ [W/m/K]	76.58
Molecular viscosity	μ [Kg/m/s]	3.446×10^{-4}
Specific heat at constant pressure	C_p [J/Kg/K]	1304.5
Prandtl number	**Pr**	5.87×10^{-3}

Table 1: physical properties of sodium at T = 300 °C

Experiment	$\bar{u}_{cf}$ [m/s]	$\bar{T}_{cf}$ [K]	Re_{cf}	$\Delta\bar{u}_j$ [m/s]	$\Delta\bar{T}_j$ [K]	ρ_j [Kg/m^3]	Re_j	Fr_j	$\dot{m}_{tot}$ [Kg/s]
A - forced jet	0.05	573	1.4×10^4	0.50	30	872.87	1.01×10^4	521	0.436
B - buoyant jet	0.1	573	2.8×10^4	0.33	25	874.05	7.9×10^3	365	0.848
C - plume	0.1	573	2.8×10^4	0.17	75	862.16	4.96×10^3	43.1	0.842

Table 2: experimental conditions.

2.2 Numerical set-up and boundary conditions

A non-uniform computational mesh of 70 × 480 cells was used, which guarantees the grid-independence of the solution [4]. A QUICK third-order convection scheme was used for the momentum and energy equations, while the Upwind first-order scheme was used for the discretisation of the turbulence equations.

Figure 2 shows the map of the boundary conditions on the computational domain. The inlet boundary condition lies in correspondence of section at x/d = 6. Profiles of the normal velocity component, as well as temperature profiles, are applied on the basis of experimental measurement in this section, using linear interpolation between the given data points.

Turbulence kinetic energy profiles are deduced by similitude with analogous experiments performed by Corrsin with air [8], namely

$$k_{Na}(r) = k_a(r)\frac{\bar{u}^2_{Na}(r)}{\bar{u}^2_a(r)}$$

where the subscripts Na and a refer to sodium and air respectively and $\bar{u}$ indicates the inlet normal velocity. This procedure, based on the similarity of the turbulence fields in the cases of sodium and air for Reynolds numbers of the same order, is the more incorrect the more buoyancy effects become important. However, it will be applied also in cases B) and C).

The problem of the inlet profile of the turbulence dissipation is more delicate, and can be considered one of the topics of the benchmark exercise. Two possible methods have been considered. The first is based on the deduction of the ε profiles from the k profiles and the relation between the turbulent viscosity, k and ε

$$\nu_t = c_\mu \frac{k^2}{\varepsilon}$$

where $c_\mu = 0.09$ and a mean value of ν_t is deduced from the air experiments with similarity considerations. The ε profiles so obtained were modified on the basis of calculations performed at FZK, in order to obtain a correct inlet momentum flux. The final ε profiles are given in [4].

An alternative is the application of the homogeneous Neumann boundary for the turbulence dissipation, extrapolating the value of the first inner cell layer onto the boundary face. This corresponds to the application of

$$\left.\frac{\partial \varepsilon}{\partial n}\right|_{inlet} = 0$$

where n is the normal to the inlet plane. In this way, the inlet values of ε are determined by the inlet profiles of u and k, with the condition of no ε flux. Although this condition is not completely correct for this case (it is correct for example for a developed boundary layer in a pipe), it could give reasonable results, also considering that the ε production term generated by the velocity gradients could be dominant with respect to the inlet ε flux.

Both solutions for the ε inlet condition have been tested.

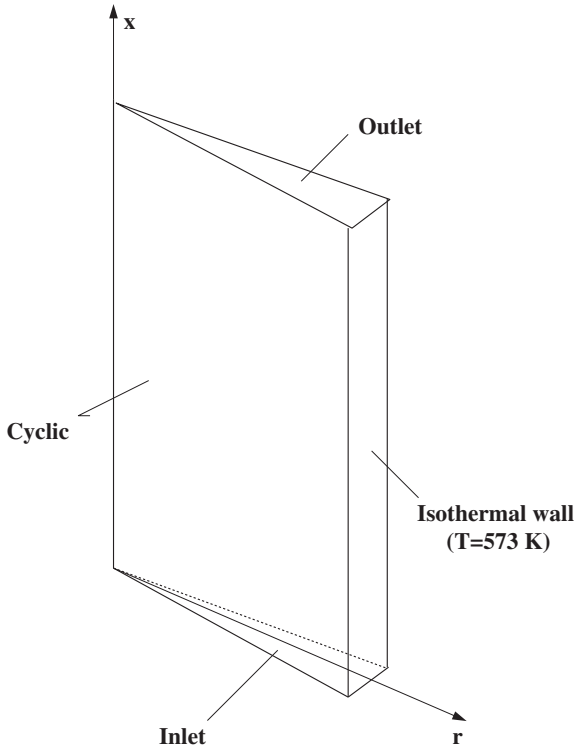

Figure 2: boundary conditions.

Concerning the inlet conditions for the turbulence parameters, the following points should be taken into account:

- the inlet profiles for the turbulence kinetic energy have been deduced from experiments performed in 1943 [8] on an air jet in stagnant fluid. The jet Reynolds number was 1.4×10^3. Some uncertainties lie in this procedure:
  - the determination of the section corresponding to the TEFLU x/d = 6 section is not straightforward (the decay of the centreline velocity is different in the two cases). Anyway, only measurements in sections at x/d = 5, 10, 15, 20, 30, 40 are reported in the Corrsin paper.
  - Detailed profiles are available only for the axial component of the velocity fluctuations. Some assumptions are necessary for the other two components.
  - The jet Reynolds number is not the same. Being relatively low, it could have an influence on the turbulence levels.
- The inlet profiles for the turbulence dissipation have been deduced using a constant mean value of the turbulent viscosity along the inlet section, and scaling the so obtained profile on the basis of numerical experiments.

Concerning the other boundaries, an outlet (imposition of mass conservation) boundary was applied in the exit section, while cyclic boundaries were applied on the side planes.

The calculations presented in this report are listed in Table 3.

	Flow regime	**Turbulence model**	**Inlet k profile**	**Inlet ε profile**	**Pr_t**
A0	forced	Chen k-ε	not scaled	imposed	0.9
A1.1	forced	Chen k-ε	not scaled	extrapolated	0.9
A1.2	forced	Standard k-ε	not scaled	extrapolated	0.9
A1.3	forced	RNG k-ε	not scaled	extrapolated	0.9
A1.4	forced	Quadratic k-ε	not scaled	extrapolated	0.9
A1.5	forced	Cubic k-ε	not scaled	extrapolated	0.9
A2.1	forced	Chen k-ε	scaled by 0.7	extrapolated	0.9
A2.2	forced	Chen k-ε	scaled by 0.7	extrapolated	10
A2.3	forced	Chen k-ε	scaled by 0.7	extrapolated	10^4
B1	buoyant	Chen k-ε	not scaled	extrapolated	10^4
B2	buoyant	Chen k-ε	scaled by 0.4	extrapolated	10^4
C1	plume	Chen k-ε	not scaled	extrapolated	10^4
C2	plume	Chen k-ε	scaled by 0.4	extrapolated	10^4

Table 3: calculation list

3 Forced-flow simulations

3.1 Comparison between the two options of extrapolated and imposed ε boundary condition

Figure 3 shows the inlet profiles interpolated on the computational mesh. The two cases of imposed (A0) and extrapolated (A1.1) ε profile (obtained in case A1.1) are shown. It can be seen that the extrapolated ε profile is very similar to the imposed one, with slightly higher values. The fact that the resulting profile of turbulent viscosity has its maximum value in the co-flow is considered reasonable, the co-flow Reynolds number being higher (implying a higher turbulence length scale).

As shown in Figure 4, the velocity and temperature axial profiles in the two cases are almost equal. However, it is the authors opinion that the extrapolation inlet ε condition is less arbitrary (especially in the cases of buoyant flow), and it has been adopted for all the successive calculations.

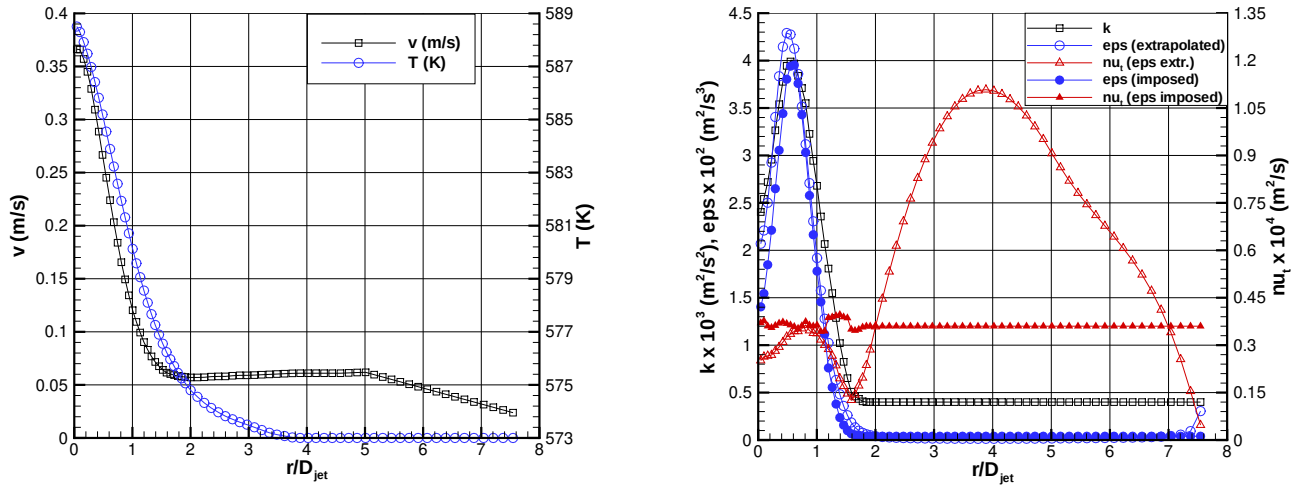

Figure 3: inlet profiles, interpolated on the computational mesh, of velocity (imposed), temperature (imposed), turbulence kinetic energy (imposed), turbulence dissipation (extrapolated for case A1.1), and turbulent cinematic viscosity (calculated from k and ε profiles).

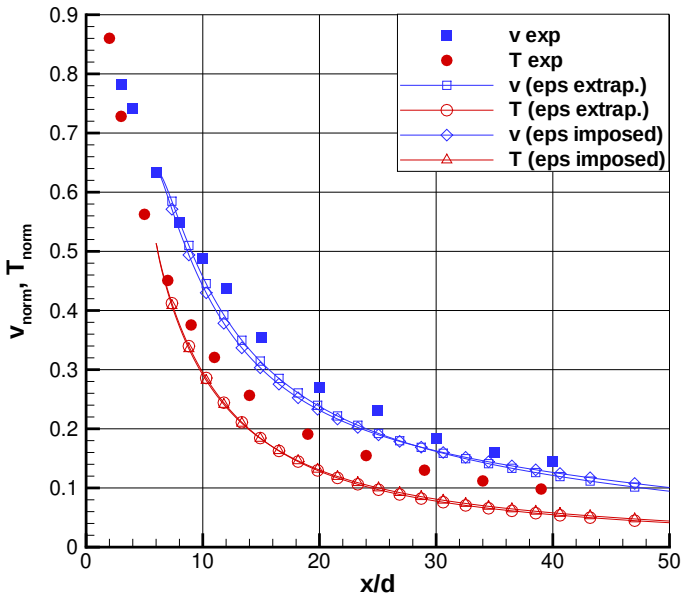

Figure 4: velocity and temperature axial profiles in the two cases of imposed and extrapolated inlet ε profile (cases A0 and A1.1).

3.2 Calculation with the Chen k-ε and comparison with other k-ε models implemented in Star-CD

The Chen k-ε [5] [6] has been chosen by the Energy Amplifier group at CRS4 as the reference turbulence model for the calculations related to the preliminary design of the Energy Amplifier Demonstration Facility. This choice was based on a brief benchmarking analysis of Star-CD capabilities on a set of standard test cases [9]. The peculiarity of this model lies in an extra term in the ε equation introducing an extra time scale of the turbulence production (in the Standard k-ε only the dissipation time scale k/ε is used). As reported in [5], this modification improves considerably the performances of the standard k-ε model in those cases where it overestimates the turbulence kinetic energy production, like round-jets.

Figure 5 and Figure 6 show the velocity and temperature axial and radial profiles obtained using the Chen k-ε (case A1.1), compared with experimental measurements. It can be seen that both velocity and temperature jet spreading-rates are under-predicted. The disagreement with experimental measurement is more evident in the case of temperature profiles.

However these results cannot be conclusive: the reason of this disagreement could lie either in a bad performance of the turbulence model or in the uncertainties in the inlet turbulence conditions.

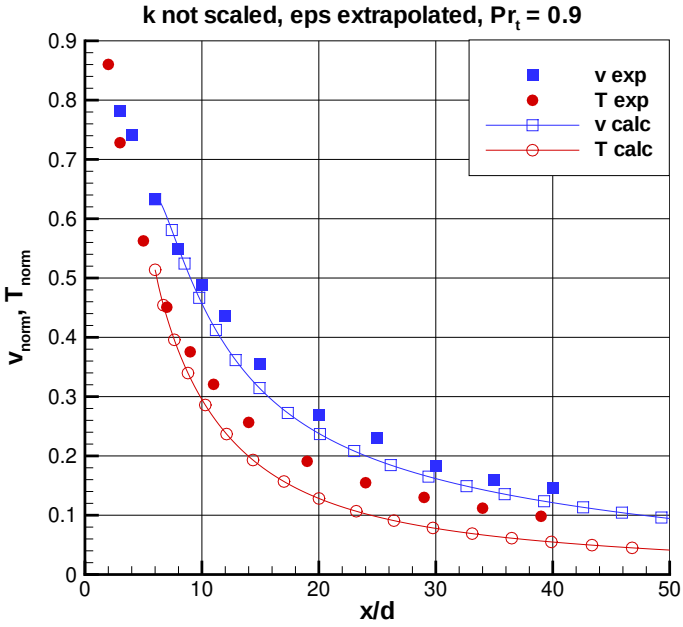

Figure 5: velocity and temperature axial profiles for case A1.1

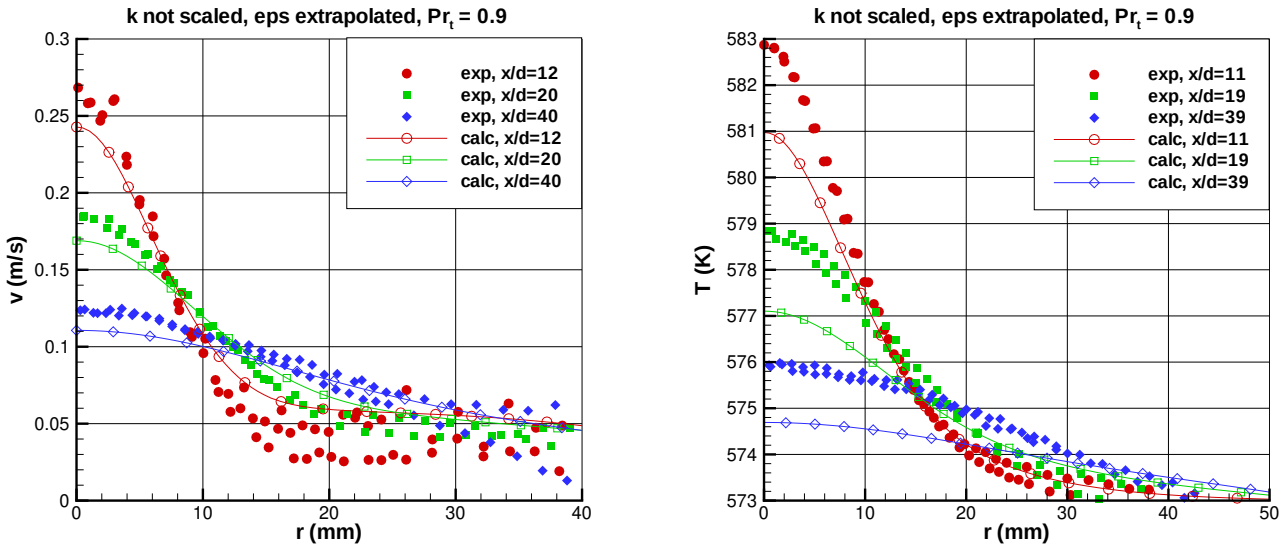

Figure 6: velocity and temperature radial profiles for case A1.1

The performances of the two-equation turbulence models implemented in Star-CD have been compared (cases A1.1-A1.5), in order to get an idea of their problems in simulating a round jet. Figure 7 shows the axial profiles of velocity and temperature. Concerning the velocity spreading-rate, it can be seen as the best results are obtained with the Chen k-ε model, followed by the Standard k-ε model. The RNG k-ε model seems to perform worse than the Standard k-ε model. The Quadratic and Cubic k-ε models, which in theory should reproduce more accurately the Reynolds stress tensor in case of flow anisotropy, give the worst results.

The quality of the prediction of the temperature spreading-rate is nearly the same for the linear models, and slightly worse in the case of the non-linear models. The agreement of the best result with experimental values is worse than in the case of velocity profiles. An explanation to these results will be given in next section.

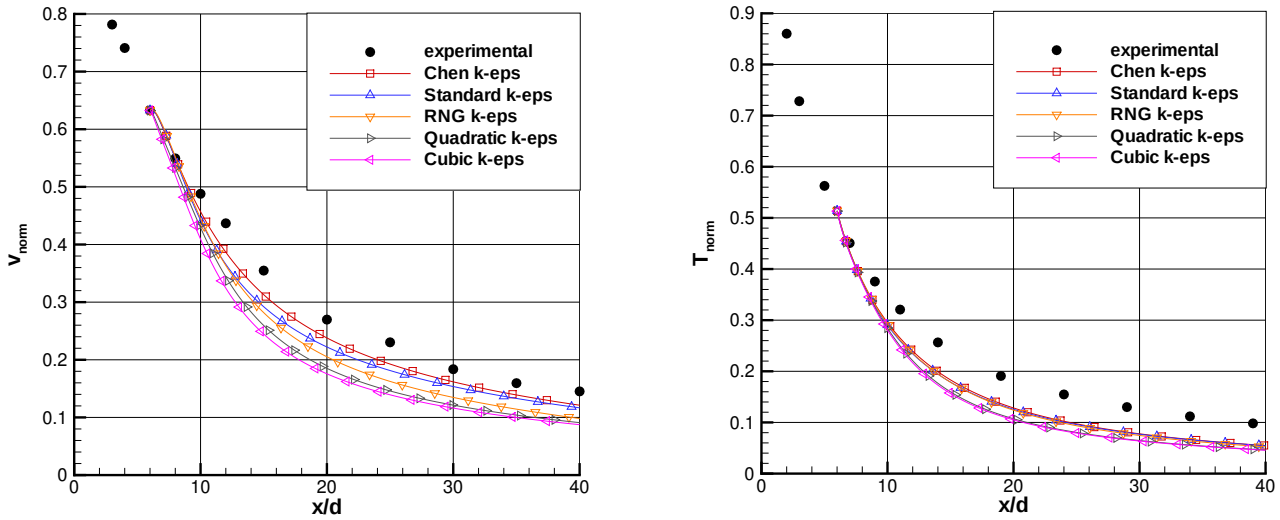

Figure 7: comparison of velocity and temperature axial profiles obtained with different k-ε models implemented in Star-CD (cases A1.1, A1.2, A1.3, A1.4, A1.5).

3.3 Analysis of the influence of the value of the turbulent Prandtl number.

In an incompressible flow where buoyancy effects are not important, the velocity field is uncoupled from the temperature field (apart from the little influence of the variation of the physical properties with temperature). In this case, also the turbulence energy and the turbulence dissipation are independent of the temperature field. Moreover, in a case like a round jet, where the flow is almost parallel, the main mechanism governing the spreading of temperature is the turbulent diffusion.

If a gradient-diffusion approach is considered applicable, this implies that, given a correct spreading rate for the velocity field, the spreading rate of the thermal field will be correctly reproduced if the turbulent diffusion coefficient

$$\lambda_t = \frac{\nu_t}{Pr_t}$$

is correct, namely, being ν_t correct, if the value of the turbulent Prandtl number is correct.

In order to obtain a velocity field in agreement with experimental results, some calculation were carried out scaling the inlet k profile by a constant (always using the extrapolation condition for ε). Figure 8 and Figure 9 show the results obtained with a scaling factor of 0.7 (axial profiles of case A1.1 are also reported for comparison). The velocity field is in good agreement with experimental data, while the temperature spreading-rate is still overestimated. This means that the turbulent diffusion coefficient is too high, namely that Pr_t is too low.

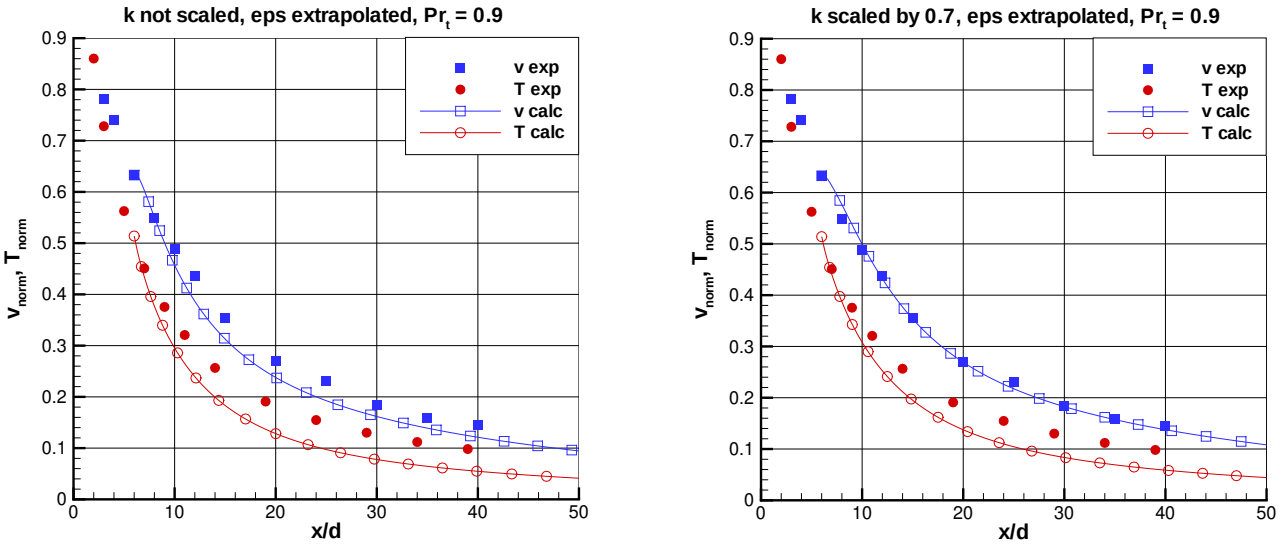

Figure 8: velocity and temperature axial profiles for cases A1.1 and A2.1

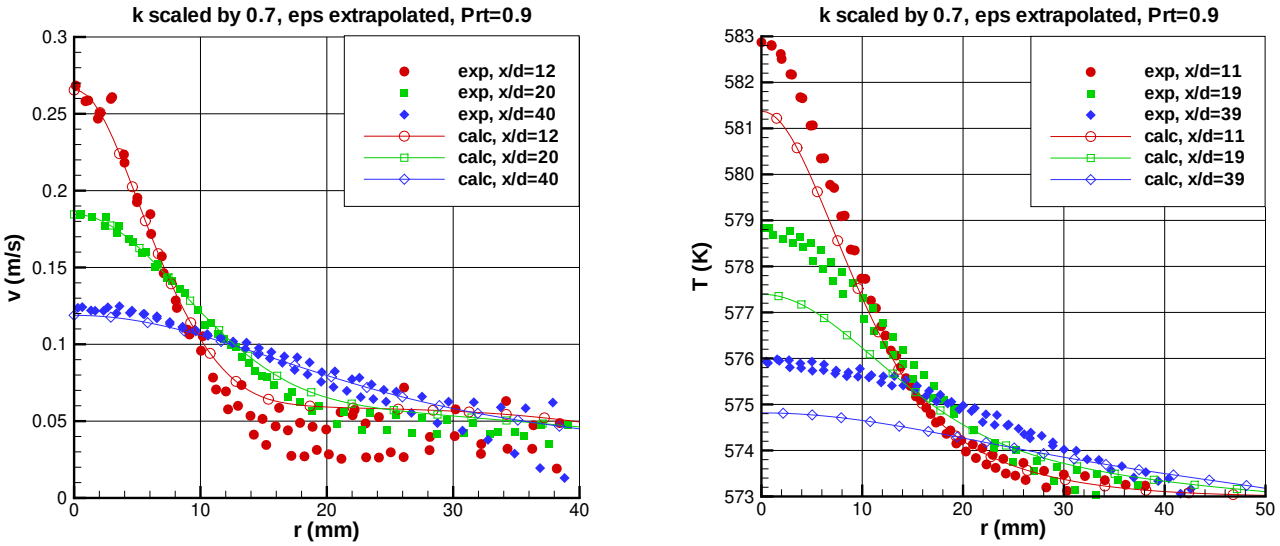

Figure 9: velocity and temperature radial profiles for case A2.1

This can be explained considering that the Reynolds analogy with a Pr_t of order 1 assumes that the mechanisms of turbulent transport of momentum and energy are the same; this is a reasonable assumption when the contribution of the molecular thermal diffusivity is of minor importance with respect to λ_t. However, This condition is not verified in our case. Figure 10 shows three radial profiles of the percentage of the turbulent conductivity with respect to the sum of turbulent and the molecular conductivity, namely

$$100\,\frac{K_t}{K+K_t}$$

where K is the thermal conductivity and

$$K_t = \rho C_p \lambda_t = \frac{C_p \mu_t}{Pr_t}.$$

This quantity gives an idea of the relative importance of molecular conduction and turbulent transport of heat. It can be seen that they are of the same order of magnitude. This is due to the combination of the very low Prandtl number of the Sodium and of the relatively low Reynolds number of the jet. In this conditions, a Pr_t of order 1 gives too much importance to the turbulent heat transport and yield to an overestimation of the total (molecular + turbulent) transport coefficient.

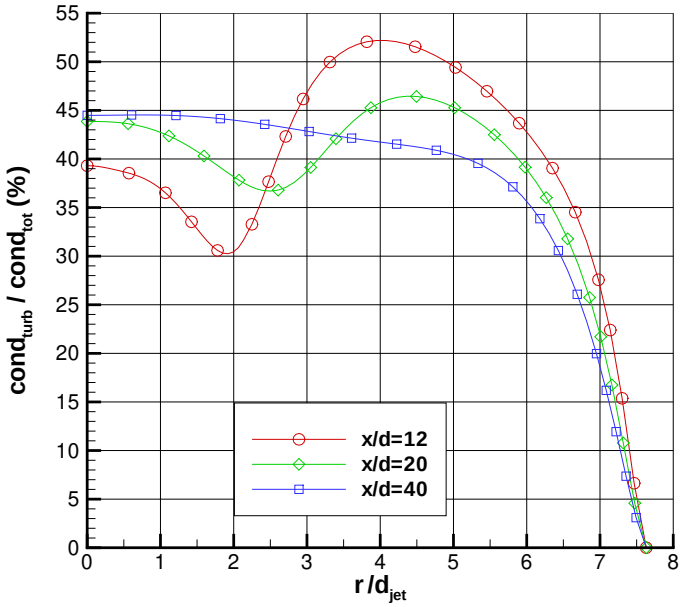

Figure 10: radial profiles of percentage of turbulent heat transport for case A2.1.

Jisha and Rieke [7], on the basis of theoretical considerations and experimental results, propose the following expression for the turbulent Prandtl number:

$$Pr_t = c_1 + c_2 \frac{1}{Pr \; Re^m}$$

$$c_1 = 0.9$$
$$c_2 = 182.4$$
$$m = 0.888$$

In our case we have $Pr = 5.87 \times 10^{-3}$ and $Re = 10^4$, yielding $Pr_t = 9.6$.

Figure 11 and Figure 12 show the results obtained using $Pr_t = 10$ (case A2.2). The agreement of temperature profiles with experimental measurements is considerably improved. However, a slight overestimation of the temperature spreading-rate can still be observed.

A further calculation was performed with $Pr_t = 10^4$ in order to make negligible the turbulent transport in the energy equation (case A2.3). As shown in Figure 13 and Figure 14, the best results

are obtained in this case. Figure 15 shows the relative importance of turbulent transport in cases A2.1, A2.2 and A2.3.

These results indicate that in the case of the forced-flow regime of the TEFLU benchmark, the only important mechanism for the heat transport is thermal conduction. In this case, a turbulent Prandtl number set to 0.9 yields an overestimation of the turbulent heat transport.

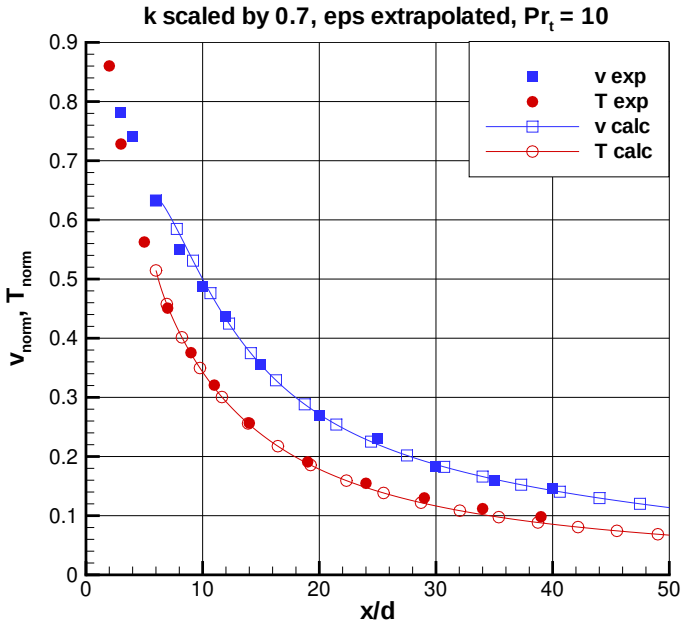

Figure 11: velocity and temperature axial profiles for case A2.2.

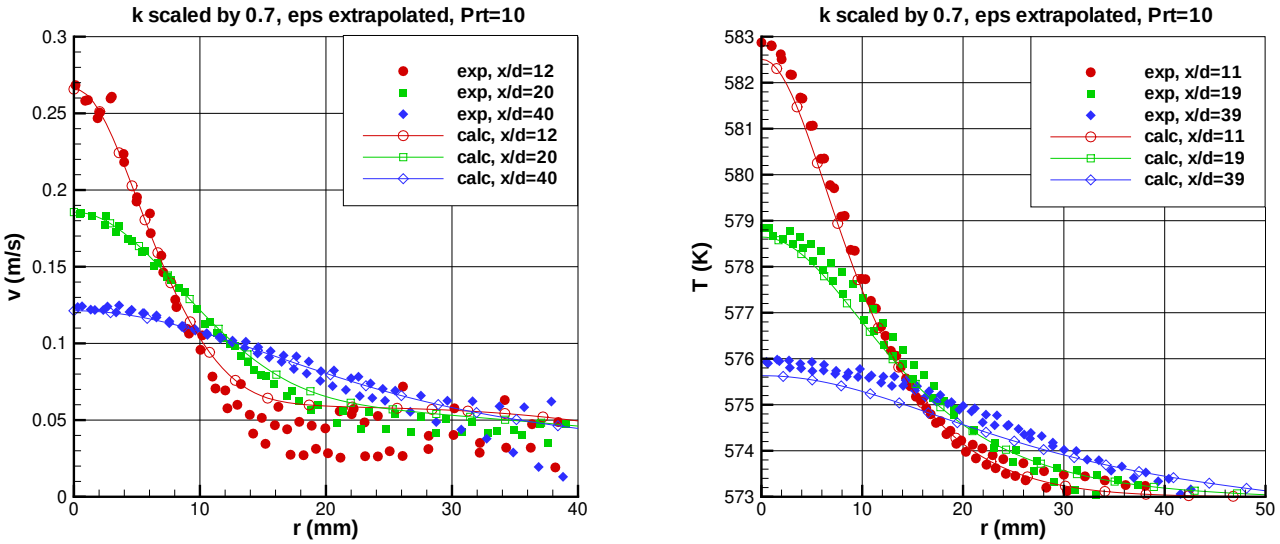

Figure 12: velocity and temperature radial profiles for cases A2.2.

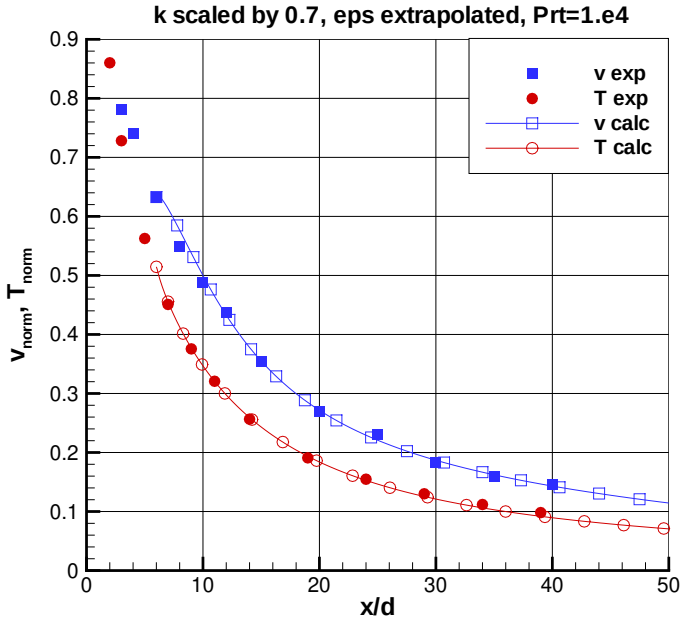

Figure 13: velocity and temperature axial profiles for case A2.3

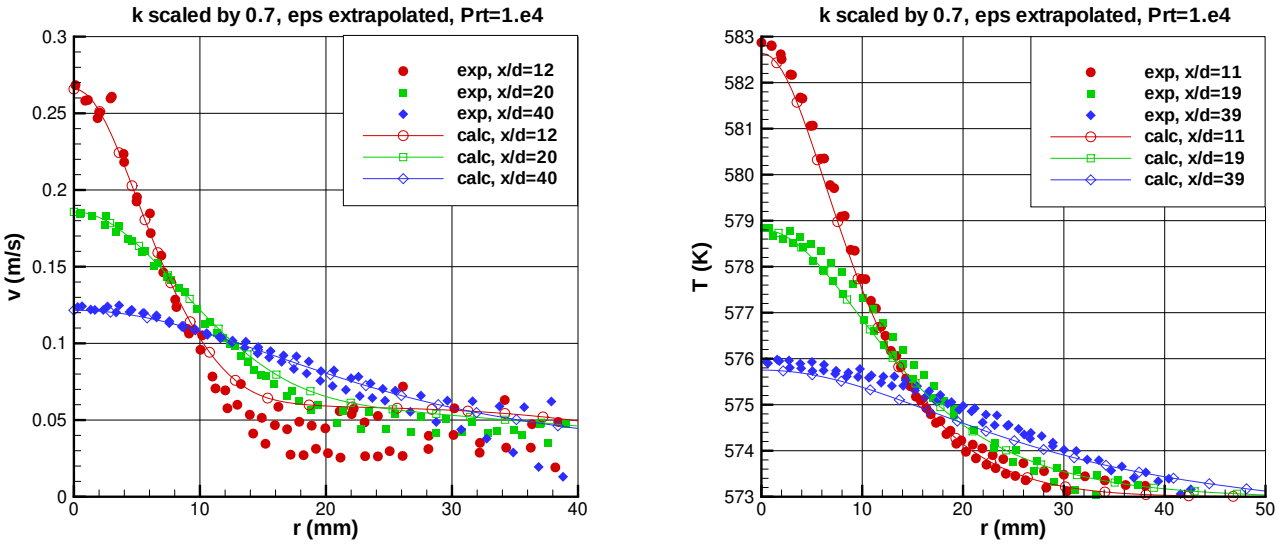

Figure 14: velocity and temperature axial profiles for case A2.3.

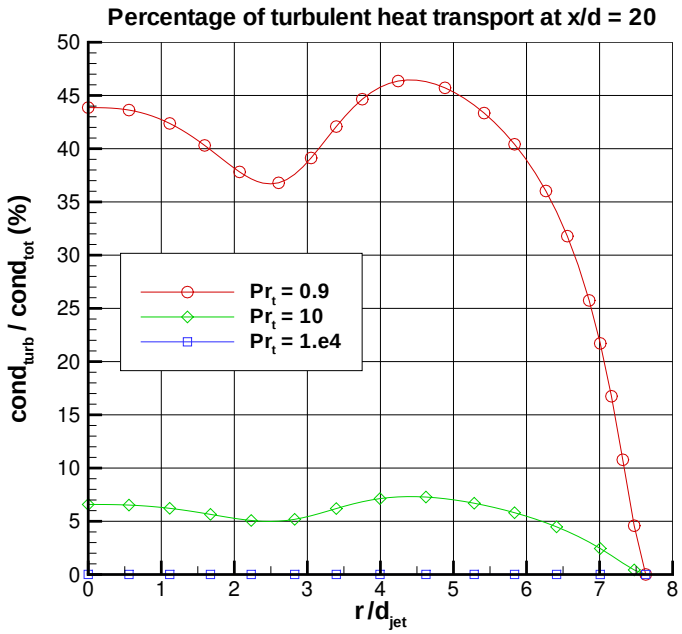

Figure 15: percentage of turbulent heat transport at x/d = 20 for cases A2.1, A2.2 and A2.3.

4 Simulations of buoyant flow and plume regimes

The simulations of the buoyant and plume regimes have been carried out on the basis of the conclusions reached in the forced-flow case. Two calculations were performed for each case: one with the k inlet profile derived by similitude from the Corrsin results, and one with the same profile scaled by a constant tuned in order to obtain a correct velocity spreading rate (always extrapolating ε), as done in the forced-flow case. In all cases the turbulent Prandtl number was set to 10^4 (so practically excluding the turbulent transport of energy).

4.1 Buoyant flow

Figure 16 and Figure 17 show the results for case B1. In spite of a strong overestimation of the velocity spreading-rate, the temperature spreading-rate is correctly reproduced. This fact demonstrates that, also in this case, the molecular thermal conductivity is the dominant phenomenon for the energy diffusion. Again, no definite conclusions can be drawn about the reasons of the bad prediction of the velocity profiles.

Figure 18 and Figure 19 show as good results can be obtained by scaling the inlet k profile by a constant factor 0.4 (case B2). With respect to the forced case, however, the shape of the axial profile is less accurately reproduced. It can be supposed that it is due to a non-correct simulation of the buoyancy effects on turbulence quantities. More reliable boundary conditions would be necessary to evaluate this aspect.

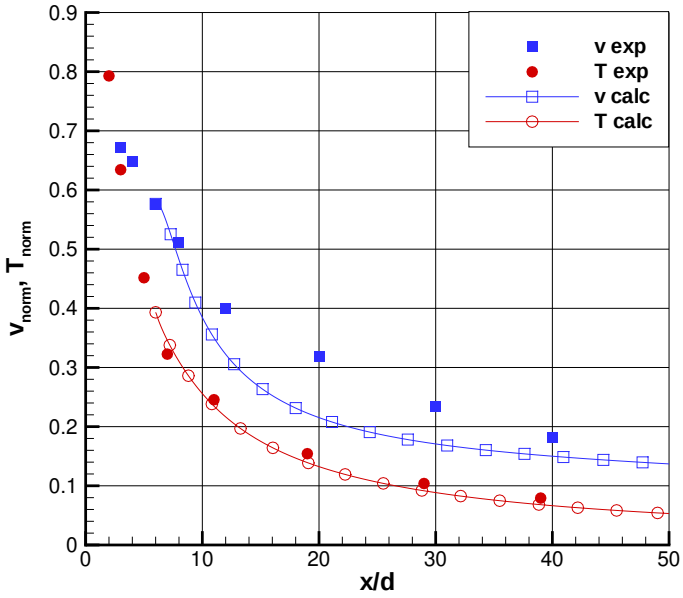

Figure 16: velocity and temperature axial profiles for case B1.

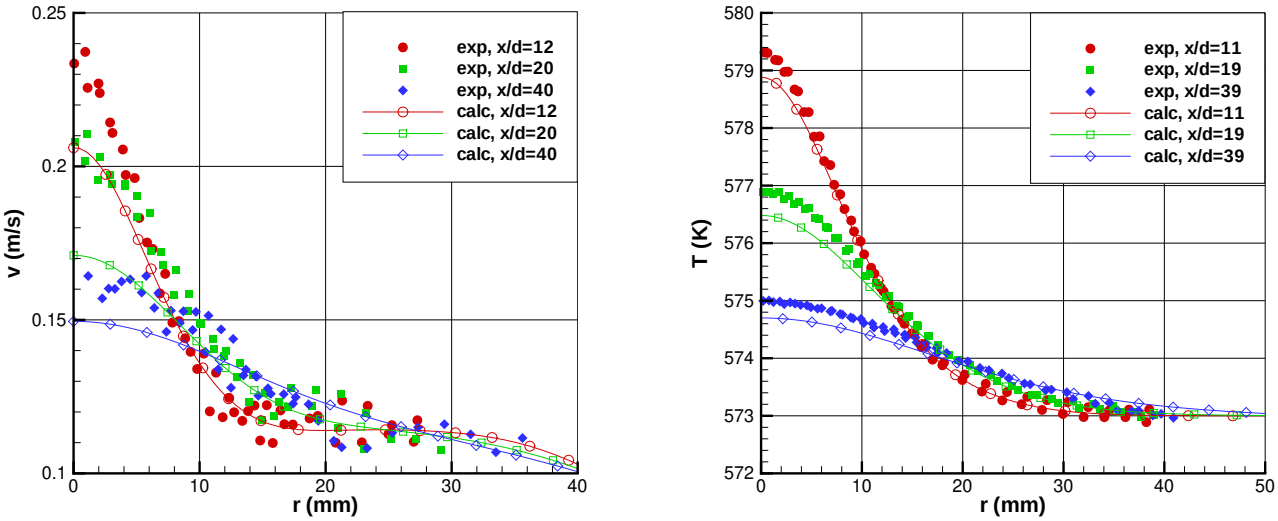

Figure 17: velocity and temperature radial profiles for case B1.

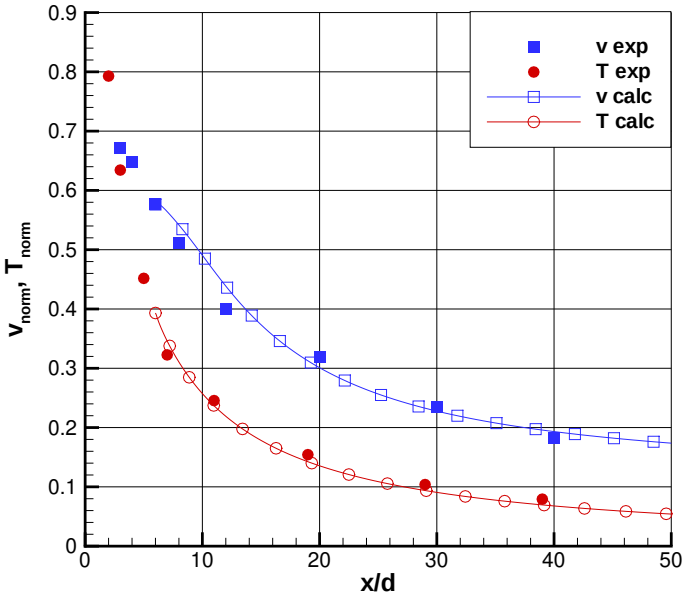

Figure 18: velocity and temperature axial profiles for case B2.

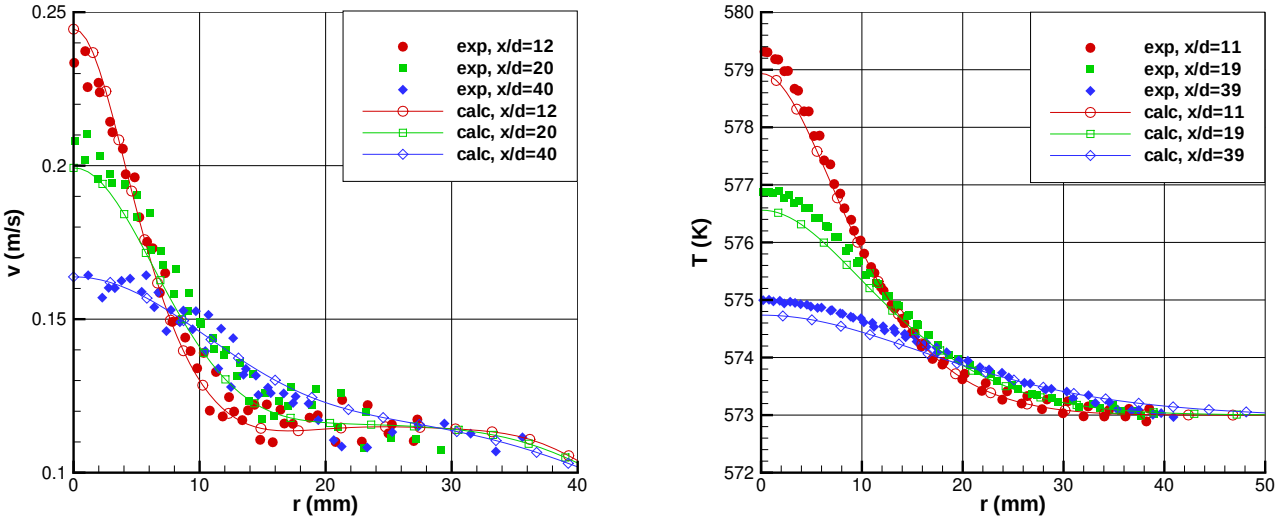

Figure 19: velocity and temperature radial profiles for case B2.

4.2 Plume

Exactly the same considerations of the previous section can be applied to the results for the plume case. It can just be noticed that the experimental uncertainty on velocity measurements is higher in this case.

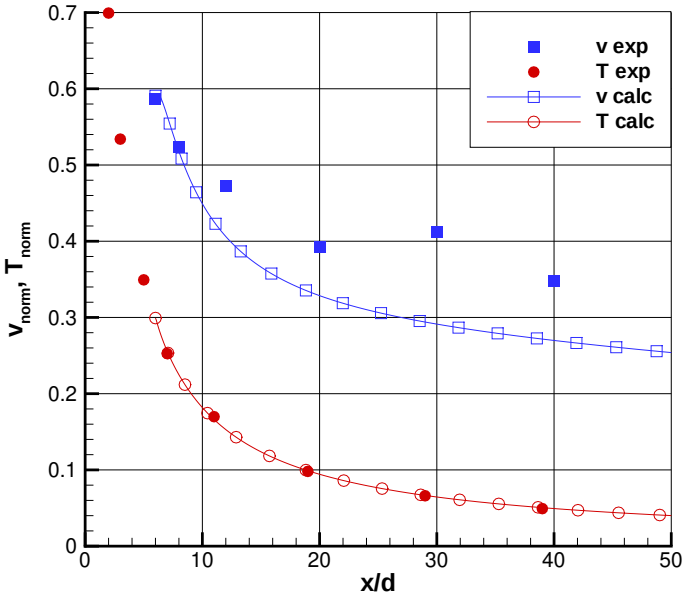

Figure 20: velocity and temperature axial profiles for case C1.

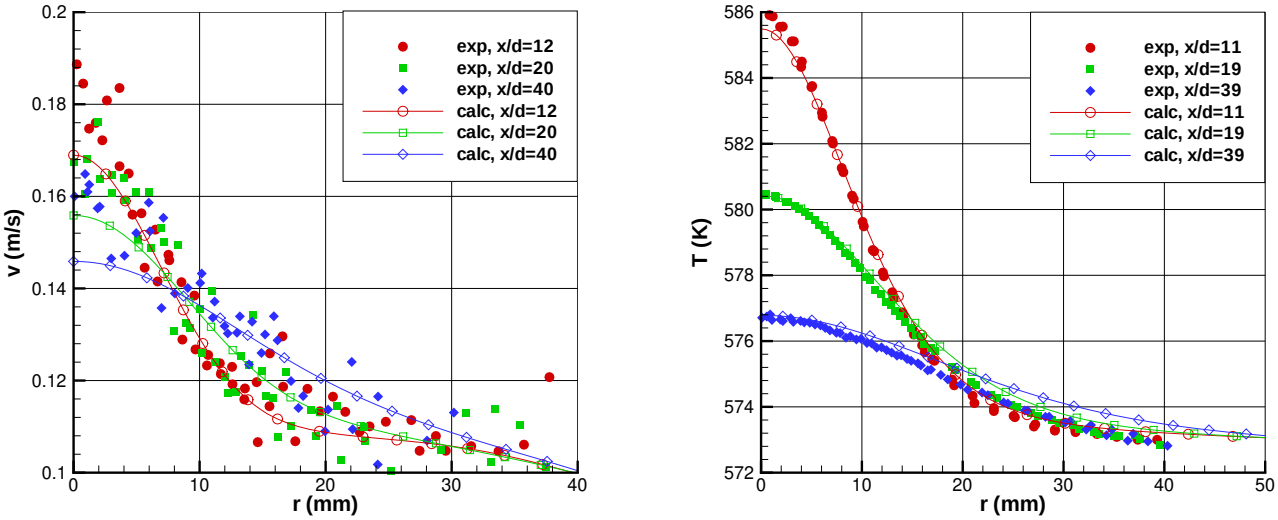

Figure 21: velocity and temperature radial profiles for case C1.

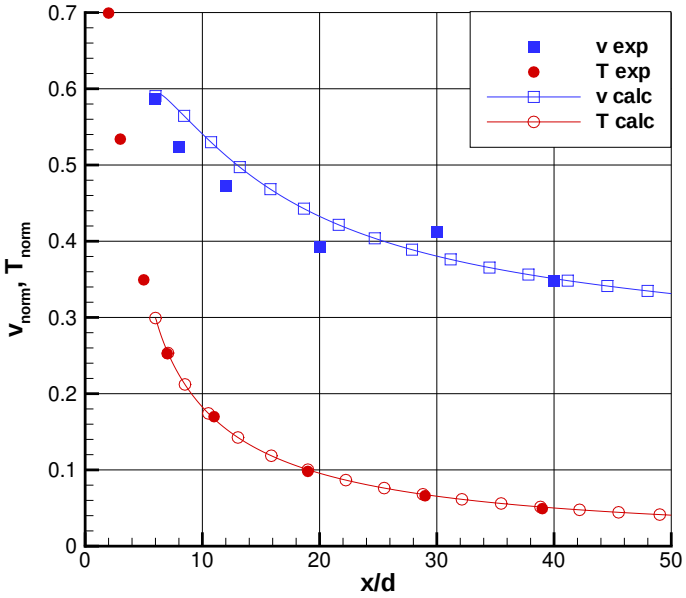

Figure 22: velocity and temperature axial profiles for case C2.

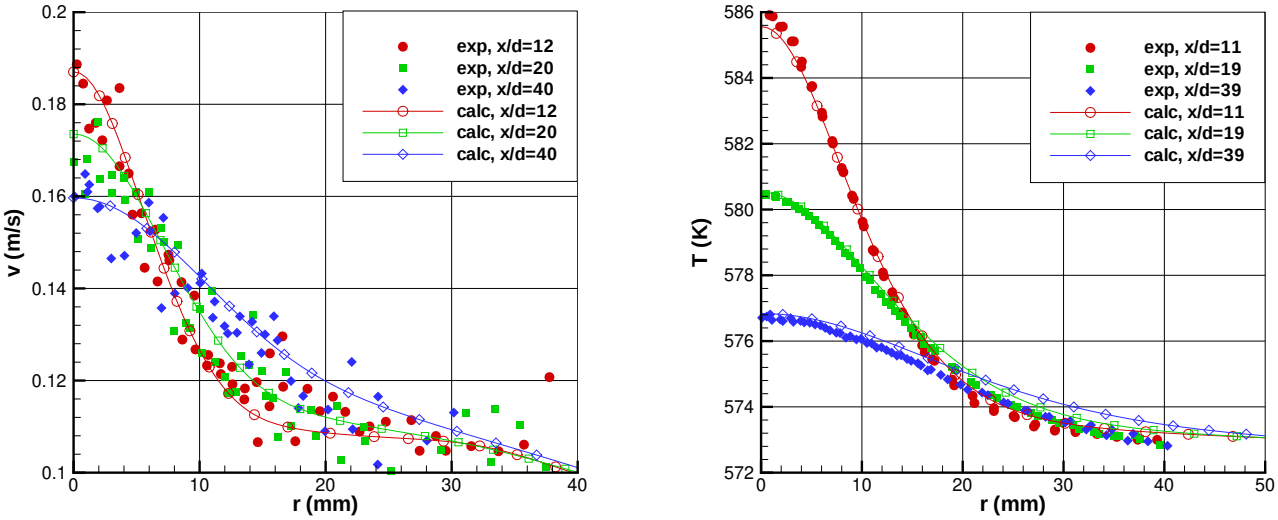

Figure 23: velocity and temperature radial profiles for case C2.

5 Conclusions

The results of the simulation of the TEFLU benchmark, obtained at CRS4 with the Star-CD code, have been reported.

Different versions of the k-ε model implemented in Star-CD have been tested. A precise answer about the capability of such models at simulating the correct jet velocity field cannot be deduced, due to the uncertainties in the inlet turbulence boundary conditions. However, the Chen k-ε showed the lowest tendency to over-predict the jet spreading-rate.